CVD-grown monolayered MoS_2 as an effective photosensor operating at low-voltage

2014 2D Mater. 1 011004

(http://iopscience.iop.org/2053-1583/1/1/011004)

2D Materials

Letter

CVD-grown monolayered MoS_2 as an effective photosensor operating at low-voltage

Néstor Perea-López[1], Zhong Lin[1], Nihar R Pradhan[2], Agustín Iñiguez-Rábago[3], Ana Laura Elías[1], Amber McCreary[1], Jun Lou[4], Pulickel M Ajayan[4], Humberto Terrones[5], Luis Balicas[2] and Mauricio Terrones[1,6]

[1] Department of Physics and Center for 2-Dimensional and Layered Materials, The Pennsylvania State University, University Park, PA 16802, USA
[2] National High Magnetic Field Laboratory, Florida State University, Tallahassee, FL 32310, USA
[3] Departamento de Física y Matemáticas, Universidad Iberoamericana, Prolongación Paseo de la Reforma 880, Lomas de Santa Fé, DF 01219, México
[4] Department of Mechanical Engineering and Materials Science, Rice University, Houston, TX 77005, USA
[5] Department of Physics, Applied Physics and Astronomy, Rensselaer Polytechnic Institute, 110 Eighth Street, Troy, NY 12180, USA
[6] Department of Materials Science and Engineering and Department of Chemistry, The Pennsylvania State University, University Park, PA 16802, USA
E-mail: mtterrrones@gmail.com

Received 12 February 2014
Accepted for publication 6 March 2014
Published 4 April 2014
2D Materials **1** (2014) 011004
doi:10.1088/2053-1583/1/1/011004

Abstract

We report the fabrication of a photosensor based on as-grown single crystal monolayers of MoS_2 synthesized by chemical vapor deposition (CVD). The measurements were performed using Au/Ti leads in a two terminal configuration on CVD-grown MoS_2 on a SiO_2/Si substrate. The device was operated in air at room temperature at low bias voltages ranging from −2 V to 2 V and its sensing capabilities were tested for two different excitation wavelengths (514.5 nm and 488 nm). The responsivity reached 1.1 mA W^{-1} when excited with a 514.5 nm laser at a bias of 1.5 V. This responsivity is one order of magnitude larger than that reported from photo devices fabricated using CVD-grown multilayered WS_2. A rectifying-effect was observed for the optically excited current, which was four times larger in the direct polarization bias when compared to the

reverse bias photocurrent. Such rectifying behavior can be attributed to the asymmetric electrode placement on the triangular MoS_2 monocrystal. It is envisioned that these components could eventually be used as efficient and low cost photosensors based on CVD-grown transition metal dichalcogenide monolayers.

Keywords: MoS_2, photocurrent, single layer

1. Introduction

Transition metal dichalcogenides (TMDs) are materials with great potential for the next generation of electronic devices. Among these, there are semiconducting TMDs that can be produced by combining the metals (M) W and Mo with the chalcogens (X) S or Se in the form MX_2. The structure of these materials consists of strong in-plane covalent bonds (X–M–X) that create isolated atomic layers that result in a bulk crystal when these sheets interact with one another through weak van der Waals forces [1–3]. Interestingly, as the number of layers is decreased their electronic properties change, with the monolayer exhibiting a direct band gap. For more than one layer, these materials reveal an indirect band gap that is kept in the bulk structure. This behavior was recently confirmed by spectroscopic and electronic means in mechanically exfoliated MoS_2 and other semiconducting TMDs [4, 5].

In mineral form, MoS_2 is the most abundant TMD (termed molybdenite) and therefore has been extensively studied when compared to other semiconducting TMDs, such as WS_2, WSe_2 and $MoSe_2$. In this context, monolayers of MoS_2 have been isolated from these mineral crystals by exfoliation through different top down approaches, including mechanical exfoliation [2, 6], chemical exfoliation [7] and ultrasonic treatments [8]. However, the use of mineral sources could introduce additional undesirable variables since the physical and chemical properties can be different from one batch to another due to the presence of unintentional dopants located at different mining sites. For this reason, research groups are now growing crystals in controlled laboratory conditions and carefully exfoliating them in order to perform different studies [9–11]. Industrial scale applications of TMDs requires the controlled growth of large areas by using bottom up approaches. So far chemical vapor deposition appears to be the most appropriate bottom up approach to synthesize monolayers of TMDs, including WS_2 and MoS_2 [12–14]. One of the most remarkable advantages of CVD is that it offers the possibility of introducing dopants as was recently demonstrated for alloys of $MoS_{2(1-x)}Se_x$, where a precise control of the band gap was achieved [15].

The semiconducting behavior of TMDs in mono- or few-layered forms has attracted great interest for the fabrication of electronic devices. Initially, field effect transistors (FETs) were produced using mechanically exfoliated monolayered MoS_2, revealing a relatively high mobility, up to 200 $cm^2\,V^{-1}\,s^{-1}$, and a very high on off ratio, up to 1×10^8 [6]. Shortly after the first reports on FETs, a MoS_2 phototransistor was built with mechanically exfoliated MoS_2 [14]. This phototransistor exhibited a photoresponsivity close to $7.5\times10^{-3}\,A\,W^{-1}$ and could be modulated by an electric field applied through the back gate [16].

The control of the flake thickness and its morphology in mechanically exfoliated samples is very poor; exfoliated samples consist of randomly oriented flakes in which single layers are

the minority. In exfoliated samples the most abundant flakes are few-layered, and several groups are exploring the electrical and optical properties of few-layered TMDs for a variety of devices, such as FETs [17, 18], phototransistors [11, 19–21] and gas sensors [22]. For example, CVD-grown few-layered WS_2 [23] was used as a photosensor capable of achieving a good response in a broad spectral range and a relatively fast response time, i.e. in the range of few milliseconds [24]. CVD synthesis constitutes a good alternative to acquire a greater control of atomic layers when compared to exfoliation. In this study we fabricate photodetectors based on CVD-synthesized monolayers of MoS_2 using a two-terminal configuration. The observed photoresponsivity indicates that the as-grown TMD monolayers can lead to the fabrication of efficient photodetectors.

2. Results and discussion

MoS_2 triangular monolayers were grown by CVD on 285 nm thick SiO_2/Si substrates using the same method previously reported for WS_2 triangular monolayered islands [12]. This method is based on the mild sulfurization of ultra-thin MoO_3 films. Figure 1(a) shows the SEM image of the device consisting of one MoS_2 triangular island connected to electrodes made of gold (Au) on titanium (Ti). A schematic representation of the monolayered MoS_2 photosensor is also presented in figure 1(b). The metal contacts were fabricated using a standard electron beam lithography technique followed by 4 nm thick Ti and 100 nm thick Au evaporations using an e-beam evaporator at 10^{-7} Torr pressure. Spectroscopic measurements performed with a confocal Raman spectrometer (Renishaw InVia™) revealed the photoluminescence (PL) spectrum presented in figure 1(c), which was acquired with a laser excitation wavelength of 488 nm. The PL spectrum has its maximum intensity at 670 nm, corresponding to a photon energy of 1.86 eV. The PL peak is slightly broader when compared to other CVD produced MoS_2; [14] its full width at half maximum is around 70 meV. Figure 1(d) shows the two first order Raman peaks of the material: the E′ peak is due to the in plane vibrational mode and the A_1' is produced by an out-of plane mode. Since the unit cell of monolayered MoS_2 is non-centrosymmetric and its vibrational modes correspond to the D_{3h} point group symmetry, the first order Raman modes should not be indexed as those observed in the bulk (E^1_{2g} and A_{1g}), which belongs to a D_{6h} symmetry [25], exhibits centrosymmetry and possesses different irreducible representations. Both the PL and Raman spectra in figure 1 were acquired in the region between the anode and cathode electrodes. The observed Raman modes confirm the presence of MoS_2 while the PL spectrum confirms the presence of monolayered MoS_2 due to the direct band gap.

The sensor response was obtained at room temperature in air using a 50× objective lens attached to the confocal Raman microscope. Two laser wavelengths were utilized in order to probe the photoresponsivities (488 nm and 514.5 nm), using a laser spot close to 2 μm in diameter. Figure 2(a) shows the bias voltage and the laser excitation in an interval between 0 s and 90 s. Figure 2(b) shows the device's total current versus time. Both plots are synchronous and the current readings were performed every 200 ms. At $t \sim 52$ s the applied bias voltage was increased from 1.5 V to 2.0 V, thus producing a barely noticeable step in the dark current. Similarly, the excitation laser was allowed to illuminate the device for 5 s starting at $t = 14$ s and $t = 64$ s. The excitation was the same in both cases (514 nm at 0.22 mW); however, the photocurrent response was around 50% larger when the bias voltage was 2.0 V ($63\ \text{s} < t < 68\ \text{s}$)

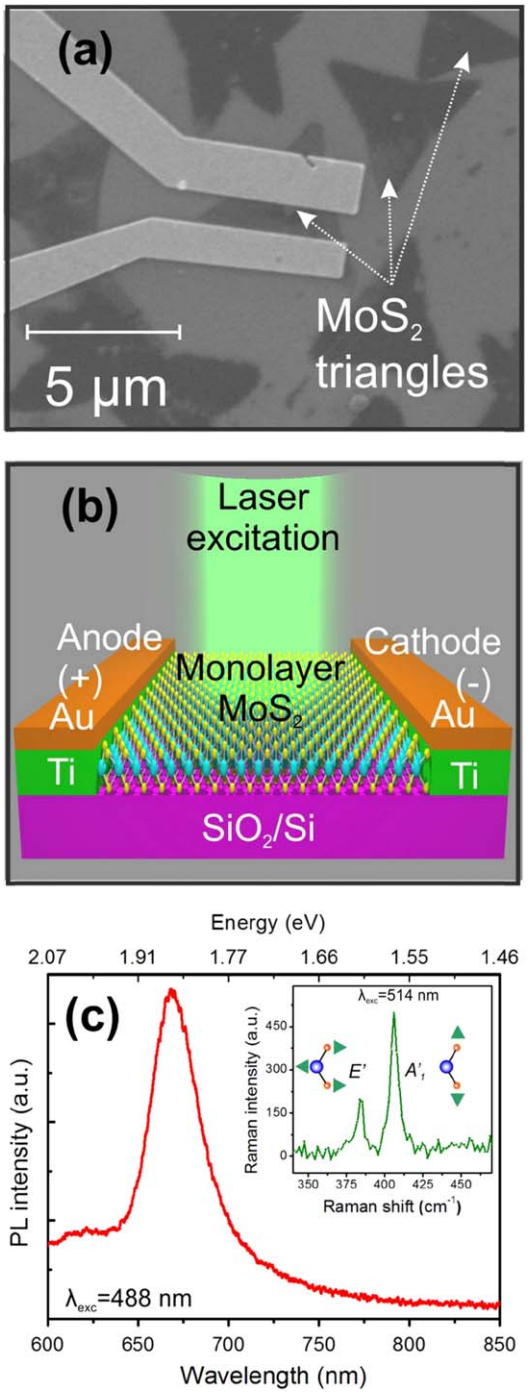

Figure 1. (a) SEM micrograph showing the CVD-grown MoS_2 triangular monolayers and the Au/Ti electrodes deposited on them by a combination of e-beam lithography and e-beam evaporation. (b) Schematic diagram of the MoS_2 monolayer photosensor depicting the electrical connections and the laser photo-excitation. (c) Photoluminescence (PL) spectrum of the active region of the MoS_2 photosensor device, whose main feature consists of a broad peak with maximum intensity located at 1.86 eV, which is associated with the PL response observed in MoS_2 monolayers. (d) Raman spectrum of monolayered MoS_2. Both spectra were acquired in the active region of the sensing device.

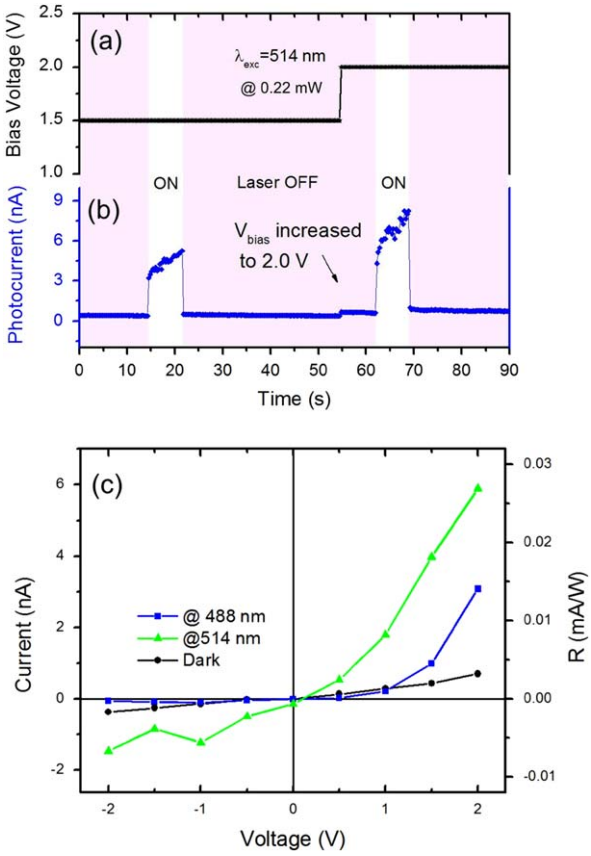

Figure 2. Variable inputs supplied to the device; (a) bias voltage and laser excitation; (b) total current as a function of time for the CVD-grown monolayered MoS_2 device. The change in the bias voltage has a strong effect on the photocurrent response, (c) *IV* plots of the device under darkness and two different wavelengths (514.5 nm and 488 nm) at the same power of 0.22 mW; a rectifying behavior is observed for the optically generated current.

when compared to $V = 1.5$ V ($14\,\text{s} < t < 19\,\text{s}$). It can also be noted that the current increases constantly whenever the laser excites the sample—this can be due to thermal effects in addition to the optically generated charge carriers [26]. In order to obtain the *IV* plots for the darkness and photocurrent components, the bias voltage was varied from −2.0 V to 2.0 V with 0.5 V steps. The obtained dark current was plotted in figure 2(c), which shows that the device is highly resistive with resistances in the range of a few GΩ. Interestingly, a slight rectifying behavior was observed in the photocurrent component for both of the used laser wavelengths. A steep increase was observed for the positive bias reaching ∼5.8 nA for 514 nm and ∼3 nA for 488 nm. Meanwhile, for the negative bias the photocurrent did not exceed ∼1.8 nA for 514 nm and it was barely measurable for 488 nm.

In the following discussion we address the mechanism for the electric current generation in TMD based devices with the metal–semiconductor–metal (M–S–M) architecture, as the one depicted in figure 3(a), in which the charge carriers have to overcome the Schottky potential barriers formed at the semiconductor–metal interfaces in order to contribute to the conduction. It is well known that the choice of the metal for the electrical contacts has a significant impact

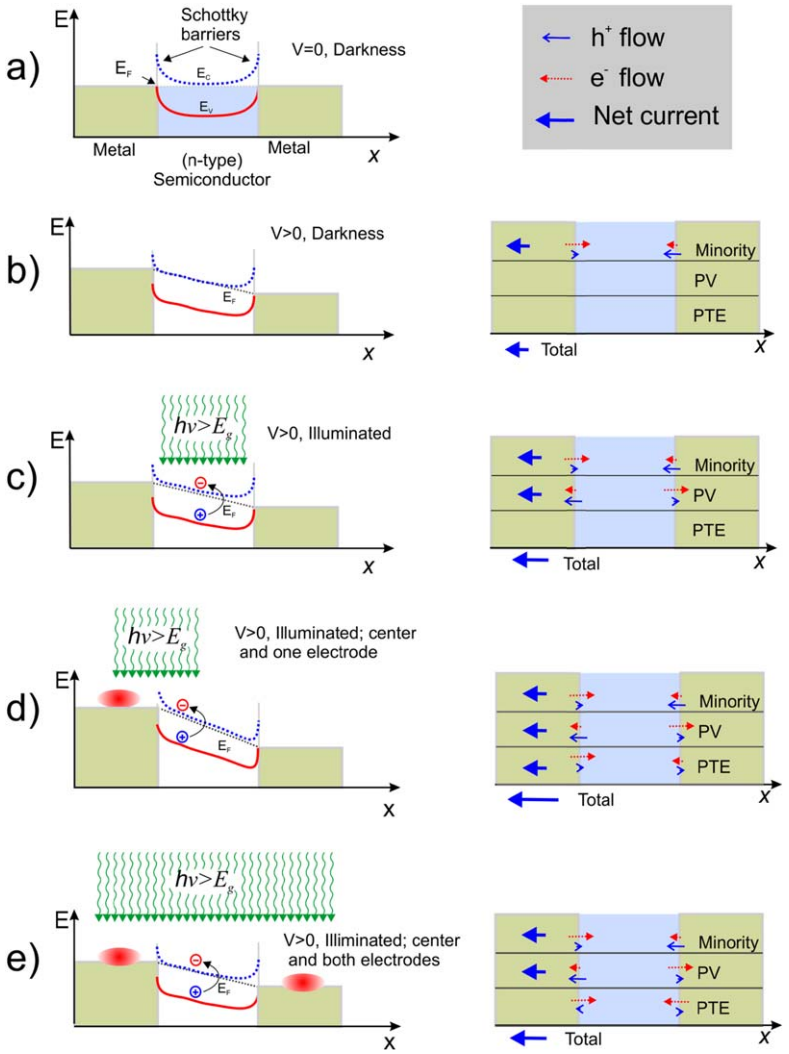

Figure 3. Schematic representations of the current generation mechanisms in a MoS_2 photosensor. (a) Energy diagram in equilibrium conditions for a metal–semiconductor–metal system and the labeling of each current component. (b) Energy diagram in darkness with an applied voltage $V>0$; the resulting current is due only to minority carriers. (c) Scenario where there is an applied voltage $V>0$ and an illumination source narrower than the semiconductor width; the current is formed by both minority and photovoltaic (PV) components. (d) The scenario where the illumination source is located in a way that excites both the semiconductor and one of the electrodes producing current through both the PV and the photothermoelectric effect (PTE) in addition to the initial current from the thermally excited minority carriers. (e) The last scenario depicts conditions similar to those of our experimental set-up, where the size of the illumination spot is wider than the semiconductor width, thus creating PTE currents on both electrodes; in such a simple scenario electron injection at each contacts cancels each other leaving only the minority and PV current components.

on the height of the Schottky barrier; in this study Ti was employed as the contact metal because its work function is similar to that of MoS_2, hence minimizing the height of the Schottky barriers [26]. There are different mechanisms of charge carrier generation involved in the electrical conduction within these devices. First, there are thermally excited minority carriers present in the semiconductor (all experiments were performed at 300 K). These carriers are responsible for the measured dark current when an external electric field is applied. (A schematic showing the components of the dark current is presented in figure 3(b).) Secondly, in direct band gap semiconductors, such as single-layer MoS_2, there are electron-hole pairs generated by a photovoltaic (PV) effect produced by photons with an energy surpassing the band gap ($E_g > 1.85$ eV). These carriers are also accelerated by the external electric field, and a schematic representing the PV mechanism is depicted in figure 3(c). The third charge carrier generation mechanism is the photothermoelectric effect (PTE) which happens at the semiconductor metal interface [26, 27]. Upon laser heating, the temperature of Au/Ti contact becomes slightly higher than MoS_2 due to their different Seebeck coefficients. This temperature difference results in a photothermal electric field in the metal–semiconductor interface. Interestingly, PTE occurs even when the energy of the photons is lower than E_g because it is induced by the absorption on the electrodes. PTE was clearly visualized by Buscema and collaborators by means of photocurrent microscopy [26]. Figure 3(d) shows a schematic of the structure where an excitation beam is placed in a way that PTE and PV carriers are created simultaneously; in this case the PTE generated electric field has the same direction as the external field, thus the total current has an added contribution from all carriers (minority, PV and PTE). However, figure 3(e) represents a scenario where the excitation beam is wider than the gap between the electrodes, and in this case, PTE generates an electric field on both metal–semiconductor interfaces, but the field produced at each interface has opposite directions, thus neutralizing each other; PTE does not contribute to the total current.

A slight rectifying behavior was observed in the *I–V* characteristics of the device whose response is shown in figure 2(c). This could possibly be due to the simultaneous occurrence of the various effects mentioned above, which in combination with the asymmetric contact area for the anode and the cathode resulted in the observed rectifying effect. In our measurements, the size of the laser spot was $\sim 2\,\mu$m in diameter, which is wider than the separation between the two electrodes ($\sim 0.8\,\mu$m), as illustrated by the schematics in figure 3(e). As a result, both the MoS_2 and the electrodes were illuminated simultaneously; hence the photothermal electric fields generated at each electrode, ideally, cancel each other, but given the asymmetry of the device and the contacts, the PTE field most likely cannot be totally suppressed. Fortunately, the contribution of each phenomenon can be discriminated since the time response for a PV related process is orders of magnitude faster than a process involving PTE because PTE is thermally driven. As a result, PTE plays a minor role in the photocurrent generation, but it is still present, as can be seen in the slow current increase observed in the current as a function of time plot in figure 2(b), during the time interval when the laser is turned on.

Figure 4(a) displays the photocurrent response as a function of the incident laser power for both of the used wavelengths. The photocurrent response is larger for the excitation wavelength of 514.5 nm (see figure 2(c)). In this set of measurements the responsivity reached 1.1 mA W^{-1}, which is almost one order of magnitude larger than the value previously reported by our group for CVD-grown multilayered WS_2 [24], being also of the same order of magnitude as the value reported for an exfoliated MoS_2 monolayer [16] and for the recently reported plasmonic nanoshells on CVD-grown MoS_2 [28]. The maximum responsivity is observed for smaller

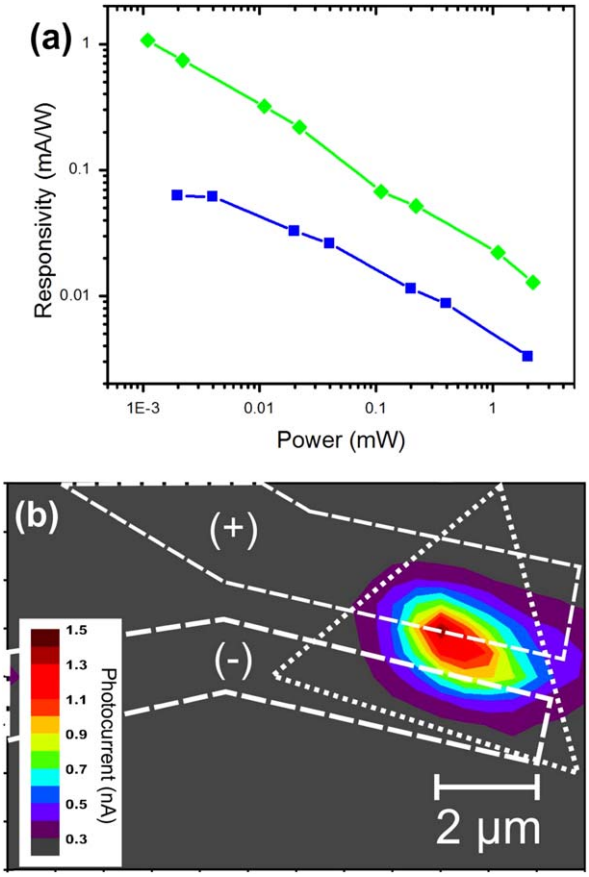

Figure 4. Photoresponse of a device based on CVD-grown monolayered MoS_2. (a) Responsivity as a function of the incoming laser power ranging from 1 μW to 2.2 mW and for both wavelengths (514.5 nm and 488 nm) when the device was operating at a constant bias voltage of 1.5 V. (b) Photocurrent map indicating the approximated location of the anode and cathode (white dashed lines). The photocurrent signal overlaps with the electrodes, but that can be an artifact since the spot size diameter (ca. 2 μm) is larger than the step size and the separation between electrodes (~0.8 μm).

incident illumination; when a small photon density reaches the semiconductor (MoS_2), all its available conduction band states can be populated so that the associated PV effect becomes more efficient under these conditions. It is noteworthy that despite its low energy, the photoresponse from the 514.5 nm (2.41 eV) excitation was around one order of magnitude larger than the one observed for the 488 nm laser line (2.54 eV). This might be caused by a larger absorption at 514.5 nm (2.41 eV), since it is closer to the new absorption peaks recently predicted theoretically and named excitons A′(2.2 eV) and B′(2.32 eV) that are present in monolayered MoS_2 [29]. Meanwhile the A exciton is located close to 1.85 eV and the B exciton at ~2.05 eV [5]. The studies of absorption in single layer MoS_2 were performed in the near vicinity of the A and B excitons [30–32].

Recently, photosensor devices reaching very high responsivity values (up to 1×10^4 A W^{-1}) were reported. Those devices have special architectures and testing conditions [33, 34]. For instance, the high gain device reported by Zhang and co-workers was achieved using large area CVD synthesized single layer MoS_2 [33]. In this design, the source and drain electrodes

had a comb like geometry and a large gate voltage (up to 90 V) was used to boost the photocurrent response. Additionally, those devices achieve high response because of their large area (in the range of 1×10^4 μm^2), which is almost four orders of magnitude larger than the area of a few μm^2 for the device discussed here. Other high gain devices were reported based on heterostructures of layered materials such as graphene/TMDs yielding a very high absorption efficiency over a broad spectral range [35]. In contrast, the responsivity of the device reported here is obtained from a two terminal configuration tested at room temperature, in air, under a bias voltage range of only ±2 V, and without the field-effect induced by a gate electrode, which leads to a strong enhancement of their photo sensitivity. It is also important to mention that in the devices reported previously it was necessary to operate at high voltages in order to obtain a high responsivity.

Finally, a photocurrent map was performed to identify the active region of the device, and for this purpose a rectangular area (12×8 μm) containing the device was scanned in steps of 0.5 μm. During the Raman mapping acquisition, a string of current as a function of time was recorded simultaneously in the Renishaw spectrometer. The laser beam scanned the sample in a raster path, starting at the top left corner and the photocurrent acquisition was performed with a Keithley™ picoammeter 6485. The current-time string was then sectioned and arranged to display a current intensity contour map. The current intensity distribution is presented in figure 4(b). A small region located between the anode and the cathode produced the highest current. When the channel length is wider than the excitation spot size, it is possible to observe the preferential generation of holes or electrons on each side of the device by PTE effect [26, 27]. Nevertheless, in our case the channel is narrower than the laser spot, and despite these mapping conditions it still allows the location of the active region in a similar way to that reported by Lopez-Sanchez *et al* [34]. From this map it is possible to show that the active region is confined to a small area between the electrodes, where the MoS_2 monolayer is located.

3. Conclusions

A low operating voltage, light sensing device was constructed with CVD-grown triangular monolayered MoS_2. The monolayered MoS_2 as the active region was confirmed by PL and Raman spectroscopy. This device exhibited a relatively high resistance of ~4 GΩ in darkness conditions, but it decreased by almost two orders of magnitude (down to 66 MΩ) when illuminated with a 514.5 nm laser beam. The maximum measured responsivity approached 1.1 mA W^{-1} but it could be further increased since the photocurrent increases steeply with the positive bias voltage. A description of the carrier generation mechanisms involved in the operation of metal–metal–semiconductor–metal devices based on single layer TMDs was presented and discussed. This work clearly demonstrates that MoS_2 monocrystalline monolayers can be used as a light sensing device at the microscopic scale with reasonable responsivity values, even without the use of a gated architecture.

Acknowledgments

This work is supported by the US Army Research Office MURI grant W911NF-11-1-0362, the Materials Simulation Center of the Materials Research Institute, the Research Computing and Cyberinfrastructure unit of Information Technology Services and Penn-State Center for

Nanoscale Science. MT thanks JST-Japan for funding the Research Center for Exotic NanoCarbons, under the Japanese regional Innovation Strategy Program by the Excellence. MT also acknowledges support from the Penn State Center for Nanoscale Science for the seed grant on 2D Layered Materials (DMR-0820404). The authors also acknowledge the Center for 2-Dimensional and Layered Materials at the Pennsylvania State University. AIR acknowledges the REU program under the NSF-DMR1062691 grant and the support from Laboratorio de Nanociencia y Nanotecnología de la Universidad lberoamericana. The authors are grateful to F Cervantes-Sodi for useful discussions.

References

[1] Joensen P, Frindt R F and Morrison S R 1986 *Mater. Res. Bull.* **21** 457–61
[2] Novoselov K S, Jiang D, Schedin F, Booth T J, Khotkevich V V, Morozov S V and Geim A K 2005 *Proc. Natl. Acad. Sci. USA* **102** 10451–3
[3] Frindt R F and Yoffe A D 1963 *Proc. R. Soc. Lond. Ser.* A **273** 69–83
[4] Splendiani A, Sun L, Zhang Y B, Li T S, Kim J, Chim C Y, Galli G and Wang F 2010 *Nano Lett.* **10** 1271–5
[5] Mak K F, Lee C, Hone J, Shan J and Heinz T F 2010 *Phys. Rev. Lett.* **105** 136805
[6] Radisavljevic B, Radenovic A, Brivio J, Giacometti V and Kis A 2011 *Nat. Nanotechnol.* **6** 147–50
[7] Eda G, Yamaguchi H, Voiry D, Fujita T, Chen M and Chhowalla M 2011 *Nano Lett.* **11** 5111–6
[8] Stengl V and Henych J 2013 *Nanoscale* **5** 3387–94
[9] Pradhan N R, Rhodes D, Zhang Q, Talapatra S, Terrones M, Ajayan P M and Balicas L 2013 *Appl. Phys. Lett.* **102** 123105
[10] Amani M, Chin M L, Birdwell A G, O'Regan T P, Najmaei S, Liu Z, Ajayan P M, Lou J and Dubey M 2013 *Appl. Phys. Lett.* **102** 193107
[11] Hwang W S *et al* 2012 *Appl. Phys. Lett.* **101** 072601
[12] Gutiérrez H R, Perea-López N, Elías A L, Berkdemir A, Wang B, Lv R, López-Urías F, Crespi V H, Terrones H and Terrones M 2012 *Nano Lett.* **13** 3447–54
[13] Lee Y H *et al* 2013 *Nano Lett.* **13** 1852–7
[14] Van der Zande A M *et al* 2013 *Nat. Mater.* **12** 554–61
[15] Gong Y *et al* 2013 *Nano Lett.* **13** 4340–5
[16] Yin Z Y *et al* 2011 *ACS Nano* **6** 74–80
[17] Das S, Chen H Y, Penumatcha A V and Appenzeller J 2013 *Nano Lett.* **13** 100–5
[18] Zhang Y J, Ye J T, Matsuhashi Y and Iwasa Y 2012 *Nano Lett.* **12** 1136–40
[19] Choi W *et al* 2012 *Adv. Mater.* **24** 5832–6
[20] Lee H S, Min S W, Chang Y G, Park M K, Nam T, Kim H, Kim J H, Ryu S and Im S 2012 *Nano Lett.* **12** 3695–700
[21] Tsai D-S, Liu K-K, Lien D-H, Tsai M-L, Kang C-F, Lin C-A, Li L-J and He J-H 2013 *ACS Nano* **7** 3905–11
[22] Late D J *et al* 2013 *ACS Nano* **7** 4879–91
[23] Elias A L *et al* 2013 *ACS Nano* **7** 5235–42
[24] Perea-López N *et al* 2013 *Adv. Func. Mater.* **23** 5511–7
[25] Terrones H *et al* 2014 *Sci. Rep.* **4** 4215
[26] Buscema M, Barkelid M, Zwiller V, van der Zant H S J, Steele G A and Castellanos-Gomez A 2013 *Nano Lett.* **13** 358–63
[27] Wu CC, Jariwala D, Sangwan V K, Marks T J, Hersam M C and Lauhon L J 2013 *J. Phys. Chem. Lett.* **4** 2508–13
[28] Sobhani A, Lauchner A, Najmaei S, Ayala-Orozco C, Wen F, Lou J and Halas N J 2014 *Appl. Phys. Lett.* **104** 031112

[29] Qiu D Y, da Jornada F H and Louie S G 2013 *Phys. Rev. Lett.* **111** 216805
[30] Shi H Y, Yan R S, Bertolazzi S, Brivio J, Gao B, Kis A, Jena D, Xing H G and Huang L B 2013 *ACS Nano* **7** 1072–80
[31] Mak K F, He K L, Lee C, Lee G H, Hone J, Heinz T F and Shan J 2013 *Nat. Mater.* **12** 207–11
[32] Newaz A K M, Prasai D, Ziegler J I, Caudel D, Robinson S, Haglund R F and Bolotin K I 2013 *Solid State Commun.* **155** 49–52
[33] Zhang W J, Huang J K, Chen C H, Chang Y H, Cheng Y J and Li L J 2013 *Adv. Mater.* **25** 3456–61
[34] Lopez-Sanchez O, Lembke D, Kayci M, Radenovic A and Kis A 2013 *Nat. Nanotechnol.* **8** 497–501
[35] Britnell L 2013 *Science* **340** 1311–4